Marine Pollution Bulletin 198 (2024) 115790

Contents lists available at ScienceDirect

Marine Pollution Bulletin

journal homepage: www.elsevier.com/locate/marpolbul

A facile approach for oil-water separation using superhydrophobic polystyrene-silica coated stainless steel mesh bucket

Rajaram S. Sutar [a], Sanjay S. Latthe [a,b,*], Akshay R. Jundle [c], Pradip P. Gaikwad [c], Sagar S. Ingole [c], Saravanan Nagappan [d], Yong Hyun Kim [e,f], Appasaheb K. Bhosale [c], Viswanathan S. Saji [g], Shanhu Liu [a,*]

[a] College of Chemistry and Molecular Science, Henan University, Kaifeng 475004, China
[b] Self-cleaning Research Laboratory, Department of Physics, Vivekanand College (Autonomous), Affiliated to Shivaji University, Kolhapur 416 003, Maharashtra, India
[c] Self-Cleaning Research Laboratory, Department of Physics, Raje Ramrao College, Affiliated to Shivaji University Kolhapur, Jath, Sangli 416404, Maharashtra, India
[d] Industry-University Cooperation Foundation, Pukyong National University, Busan 48513, Republic of Korea
[e] Department of Smart Green Technology Engineering, Pukyong National University, Busan 48513, Republic of Korea
[f] School of Electrical Engineering, Pukyong National University, Busan 48513, Republic of Korea
[g] Interdisciplinary Research Center for Advanced Materials, King Fahd University of Petroleum & Minerals, Dhahran 31261, Saudi Arabia

ARTICLE INFO

Keywords:
Oil-water separation
Polystyrene-SiO_2
Superhydrophobic
Stainless steel mesh

ABSTRACT

Inspired by traditional shaduf technology in the irrigation field, we fabricated a superhydrophobic stainless steel mesh bucket by layering polystyrene and SiO_2 nanoparticles through a facile dip coating technique for effective oil-water separation. The superhydrophobic steel mesh bucket could effectively lift oil as well as microplastic pollutants from the water surface. The water contact angle of a two-layered polystyrene-silica coating was 158.5° ± 2°, while the oil contact angle was nearly 0°. The oil-water separation performance of superhydrophobic mesh was tested using several kinds of oil. The separation efficiency achieved for low viscous oil was 99.33 %, while 86.66 % efficiency was recorded for high viscous oil. The superhydrophobic mesh showed high durability against mechanical tests including bending, folding, twisting, adhesive tape tearing (25 cycles), and sandpaper abrasion (20 cycles). The mesh presented admirable thermal and chemical durability. The present superhydrophobic steel mesh bucket is a suitable candidate for large-scale application.

1. Introduction

Frequently occurring oil spill accidents and continuous discharging of oily industrial wastewater are warning threats to the environment, the sea ecosystem and human health (Barron et al., 2020; Jung et al., 2017). The separation of oil and water to dispose of oily wastewater is a global issue. Traditional methods for oil-water separation are neglected due to their low efficiency, time consumption, and cost (Gong et al., 2018; Gupta and Tai, 2016; Saththasivam et al., 2016). Special wetting surfaces, such as superhydrophobic/superoleophilic and superhydrophilic/superoleophobic, have piqued the interest of academics, researchers, and manufacturers during the past decade. Surfaces that are superhydrophobic/superoleophilic repel water and absorb oil (Baig et al., 2022; Guo et al., 2018; Lü and Lin, 2021; Wang et al., 2019; Zhou et al., 2021a), whereas superhydrophilic/superoleophobic surfaces absorb water and repel oil (Chen et al., 2023; Li et al., 2022; Pan et al., 2018; Qu et al., 2018; Xiong et al., 2021; Zarghami et al., 2019; Zhou et al., 2021b).

Superhydrophobic surfaces possess the potential for achieving remarkable water-repelling properties by exhibiting high water contact angles (WCA) and low water sliding angles (SA) or lower contact angle hysteresis (CAH) (Dalawai et al., 2020). The contact angle of a water droplet on a solid surface (the angle between the solid surface and the tangent of a water drop) is influenced by the chemical and structural composition of the surface. While chemical composition with low surface energy of solid surface is fixed, roughness can alter contact angle. Conversely, while the roughness of a solid surface is fixed, low surface energy chemical modification can vary the contact angle. Water droplets roll off from a superhydrophobic surface when inclined by a small angle (<10°), known as the SA. The tilted plate method is typically used to measure SA (Yao et al., 2020; Ji et al., 2018). The method involves placing a droplet on a level surface and then gradually tilting until the

* Corresponding authors at: College of Chemistry and Molecular Science, Henan University, Kaifeng 475004, China.
E-mail addresses: latthes@gmail.com (S.S. Latthe), liushanhu@vip.henu.edu.cn (S. Liu).

https://doi.org/10.1016/j.marpolbul.2023.115790
Received 10 August 2023; Received in revised form 10 November 2023; Accepted 11 November 2023

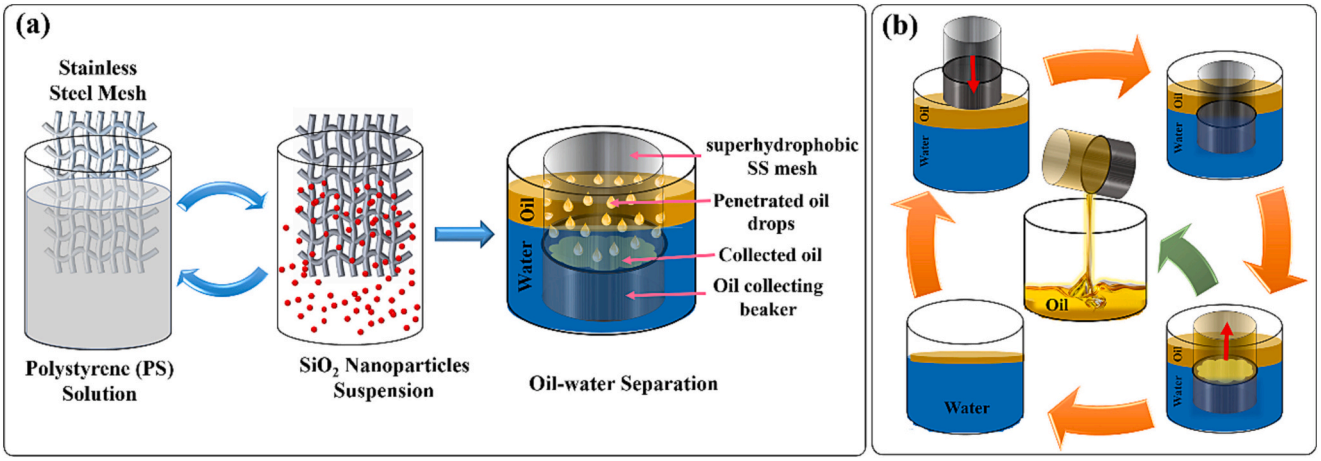

Fig. 1. (a) Schematic diagrams illustrating the process of creating a superhydrophobic steel mesh and (b) using it for oil-water separation in a mesh bucket.

droplet slides. The CAH is the difference between the advancing and receding contact angles; the difference is <10°, which can be determined by the tilted plate method (Wang et al., 2015). On an inclined surface, the angles at the leading and trailing edge of a drop profile are known as the advancing and receding contact angles, respectively. The water droplets do not stick to a self-cleaning superhydrophobic surface, resulting in a WCA > 150° and SA or CAH < 10°.

Over the past decade, various nanoparticles such as SiO_2, TiO_2, and ZnO have been used along with polymers to alter the surface wettability of porous metal meshes, textiles, and sponges (He et al., 2022; Kumari et al., 2022; Latthe et al., 2019; Li et al., 2020; Phan et al., 2021; Ren et al., 2023; Velayi and Norouzbeigi, 2020). Various methods have been utilized to deposit nanoparticles-based composites on porous substrates, including dip (Bolvardi et al., 2019), spray (Hwang et al., 2011), sol-gel (Xiu et al., 2008), chemical vapor deposition (Xu et al., 2018), electrospray (Song, 2016), and layer-by-layer (Zhang et al., 2007). Among the porous substrates, stainless steel mesh has high liquid permeability, durability, flexibility, and exhibits microscale roughness. As a result, the surface may readily create superhydrophobic wetting by depositing low surface energy or hydrophobic material. This has proved to be an effective way to separate oil, dyes, salts, heavy metals, organic pollutants and microplastics from water mixture (Sajid et al., 2022; Rius-Ayra et al., 2022a; Guo et al., 2020; Li et al., 2017; Rius-Ayra et al., 2022b; Rius-Ayra et al., 2022c).

Guo et al. (2020) used a dip coating approach to apply sol-gel processed oleophilic/hydrophobic silica sol to stainless steel mesh. The coated mesh showed >95 % of oil separation rate with a WCA of 157°. Li et al. (2017) made a superhydrophobic stainless steel mesh by spraying a mixture of water-resistant polyurethane and silica nanoparticles. After 40 cycles of oil-water separation, this superhydrophobic mesh separated up to 98 % of the oil from water. Latthe et al. (2019) have developed a superhydrophobic leaf mesh by depositing a dipping layer of SiO_2-polystyrene nanocomposite on the naturally dried surface of *Tectona grandis* leaves. The superhydrophobic leaf mesh had a separation efficiency >95 % for over 18 separation cycles. Recently, a few studies showed that porous materials with superhydrophobic/superoleophilic characteristics can facilitate the separation of microplastics from water surfaces. Rius-Ayra et al. (2022b) have prepared superhydrophobic stainless steel mesh by chemical etching and subsequent low surface energy polydimethylsiloxane modification. Superhydrophobic mesh achieved 99 % hexane oil separation and removed 2.8 mg of high-density polyethylene microplastics per 1 mL of water. In another work, stainless steel mesh was subjected to chemical etching and lauric acid modification and the fabricated superhydrophobic/superoleophilic mesh exhibited WCA of 169° and oil contact angle (OCA) of 0°. The separation efficiency of the modified mesh for microplastic removal was 99 ± 0.5 % (Rius-Ayra et al., 2022c).

Previous literature has shown that the wetting properties of mesh and membrane materials can be improved by depositing nanocomposites. Oil and water separation processes typically rely on gravity-driven or filtration methods, which have some limitations. These include the need for complex separation device designs, device installation in a vertical or inclined position, poor sustainability of mesh and membrane materials, and the requirement to pour oil-water mixtures into a pre-designed upper container and collection in an underneath container. Additionally, these methods require the separation of a pre-fixed volume of the oil-water mixture. However, the operational process of separating oil-water mixture and designing the necessary devices is quite complicated. There is an urgent need for simple and efficient technology to separate oil-water mixture effectively.

In this work, we used a facile dip coating method to deposit a layer of polystyrene (PS) and SiO_2 nanoparticles to fabricate a superhydrophobic/superoleophilic stainless steel mesh bucket. The bucket design draws inspiration from traditional shaduf technology used in irrigation. The surface and chemical properties of the coating were studied by SEM, EDS and FTIR. The oil-water separation performance of the mesh bucket was investigated using several types of oil-water mixtures. We have used traditional technology to separate oil as well as microplastics from water. In future research, exploring peristaltic pump-operated technology for continuous oil-water separation would be beneficial.

2. Experimental

2.1. Materials

Polystyrene (PS; 192,000 g/mol, pellet size: 4–5 mm, Sigma-Aldrich), hydrophobic SiO_2 nanoparticles (AEROSIL RX 300-5, Surface area: 180–210 m^2/g, particle size: 75–83 nm), chloroform (99 %, Sisco Research Laboratories), and hexane (Puriss, Spectrochem, India) were used. 316-Stainless steel mesh (Mesh size: 400 and thickness: 25.4 μm) was purchased from Shanghai Titan Technology Co., Ltd., China. The petrol, kerosene, diesel (BPCL, India), coconut oil (Parachute Advanced, India) and vegetable oil (Saffola Gold, India) were used to test oil-water separation.

2.2. Fabrication of superhydrophobic stainless steel mesh bucket

Commercially available stainless steel mesh was cut into 4 × 4 cm^2 squares. Primarily, the mesh was cleaned by water and ethanol multiple times to remove surface contaminants. The washed meshes were thoroughly dried in hot air oven at 70–80 °C for 10 min. The PS solution was

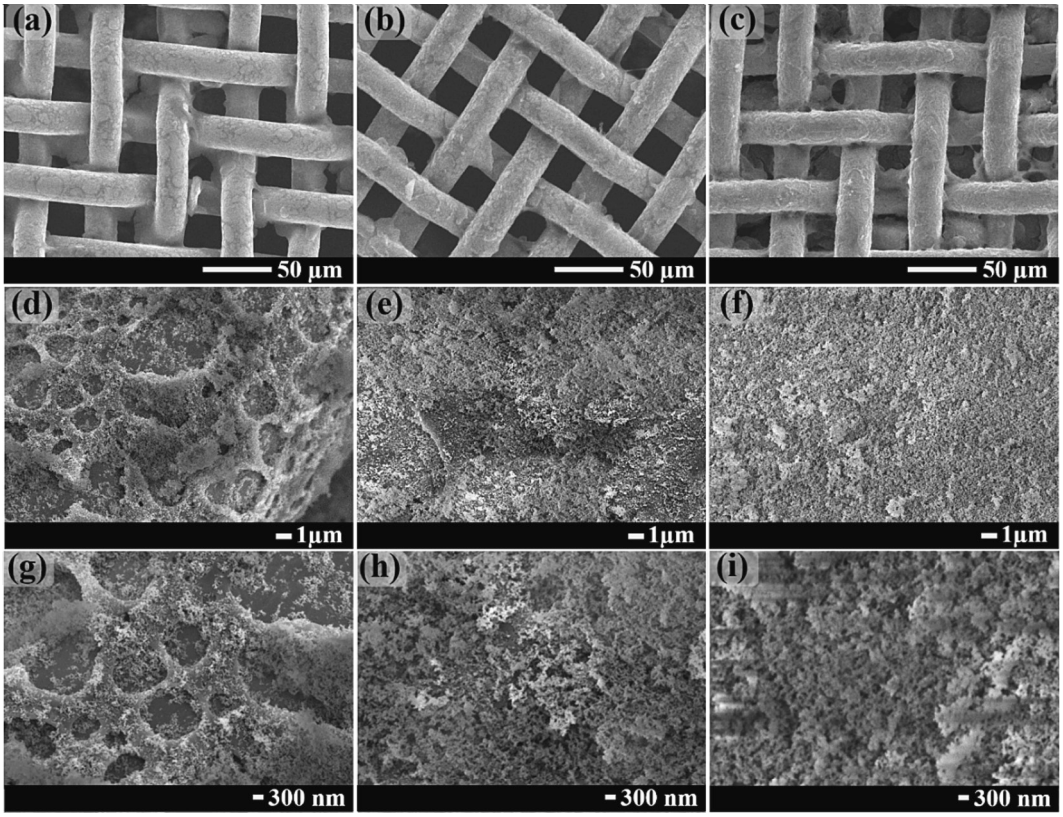

Fig. 2. SEM micrographs of (a) SS-1, (b) SS-2 and (c) SS-3 samples. Magnified SEM micrographs of (d, g) SS-1, (e, h) SS-2 and (f, i) SS-3.

made by dissolving PS into chloroform in a volume ratio of 0.4 g / 40 mL and stirring it with a magnetic stirrer at a constant speed of 150 rpm for 1 h. Meanwhile, in another beaker, 0.8 g of SiO_2 nanoparticles were disseminated in 40 mL of hexane using a magnetic stirrer set to 150 rpm and stirred for 1 h. The cleaned mesh was initially immersed for 5 min in the prepared PS solution. The mesh was then removed and dried at room temperature for 10 min. The PS layer deposited mesh was dipped in SiO_2 nanoparticles dispersion for 5 min, removed and heated in air at 80 °C for 1 h. Further, the coating process was repeated multiple times (maximum 3 times). The mesh coated with one, two, and three sequential layers of PS and SiO_2 nanoparticles were designated as the SS-1, SS-2, and SS-3 samples, respectively. The as-prepared samples were used for characterization studies. Two-time coated (two sequential PS and SiO_2 nanoparticle layers) 16.5 × 3 cm^2 sized stainless steel meshes were used to prepare the mesh bucket. A similar coating procedure as described above was used. The as-fabricated mesh was fixed on a 100 mL cylindrical plastic bucket using highly adhesive cyanoacrylate glue (obtained from Pidilite Industries Ltd., India). The cylindrical plastic bucket had an outer diameter of 5 cm; therefore, the prepared mesh bucket acquires the same diameter as the plastic bucket. Fig. 1a and b, respectively, show schematic diagrams of the steps involved in making the superhydrophobic mesh and the oil-water separation using the mesh bucket.

2.3. Characterizations

Scanning Electron Microscopy (SEM, JEOL, JSM-7610F), Energy Dispersive Spectroscopy (EDS, JEOL, JSM-6360A), and Fourier-Transform Infrared Spectroscopy (FTIR) were used to analyze the surface and chemical structure of the coated steel meshes. The wetting characteristics were investigated through a contact angle meter (HO-IAD-CAM-01, Holmarc) to measure the WCA, OCA, and SA. The mesh was affixed to a glass micro slide with double-sided adhesive tape. Then, it was placed on the sample stage of the contact angle meter. The water/oil drop was deposited on the coated mesh using a syringe for measuring the WCA/OCA. To measure the SA, the tilting plate method was used. A water droplet (20 μL) was placed on the coated mesh. The sample stage is then tilted to allow the droplet to roll down the mesh surface. Various oil and water mixtures were used to evaluate the oil-water separation capacity of the superhydrophobic stainless steel mesh bucket. When the bucket was submerged in an oil-water mixture, oil passed through the steel mesh, and the oil was collected in the plastic bucket designated for oil collection. Then, the bucket was removed, and the oil was poured into a another glass beaker. This process was repeated up to three times to completely separate the oil-water mixture. Polyvinyl chloride (PVC) microparticles (particle size 100 ± 25 μm) were used to determine the microplastic removal ability of the mesh bucket. The mechanical rigidity of the coatings was evaluated by several times bending, folding, and twisting the mesh. An abrasion test using 320 grit sandpaper and a tape peeling test with 4 N/m adhesive tape were also performed. Thermal stability was assessed by heating the mesh to 300 °C and placing hot water on it. The chemical stability of coatings was studied by immersing coated mesh in the different pH solutions for 10 days.

3. Results and discussion

3.1. Surface and elemental analysis of coatings

Fig. 2 depicts the SEM micrographs of coated steel meshes. The variation of morphology after the PS-SiO_2 coating is evident. Silica nanoparticles become agglomerated in polymer networks and are unevenly distributed over the initial PS-SiO_2 layer (SS-1). The coating of PS and SiO_2 altered the smooth surface structure of the mesh. The surface roughness of the coating was induced by aggregated silica nanoparticles (Fig. 2a). It can be seen in Fig. 2d that the initial PS-SiO_2 layer forms a network-like structure with several gaps. Its magnified image reveals

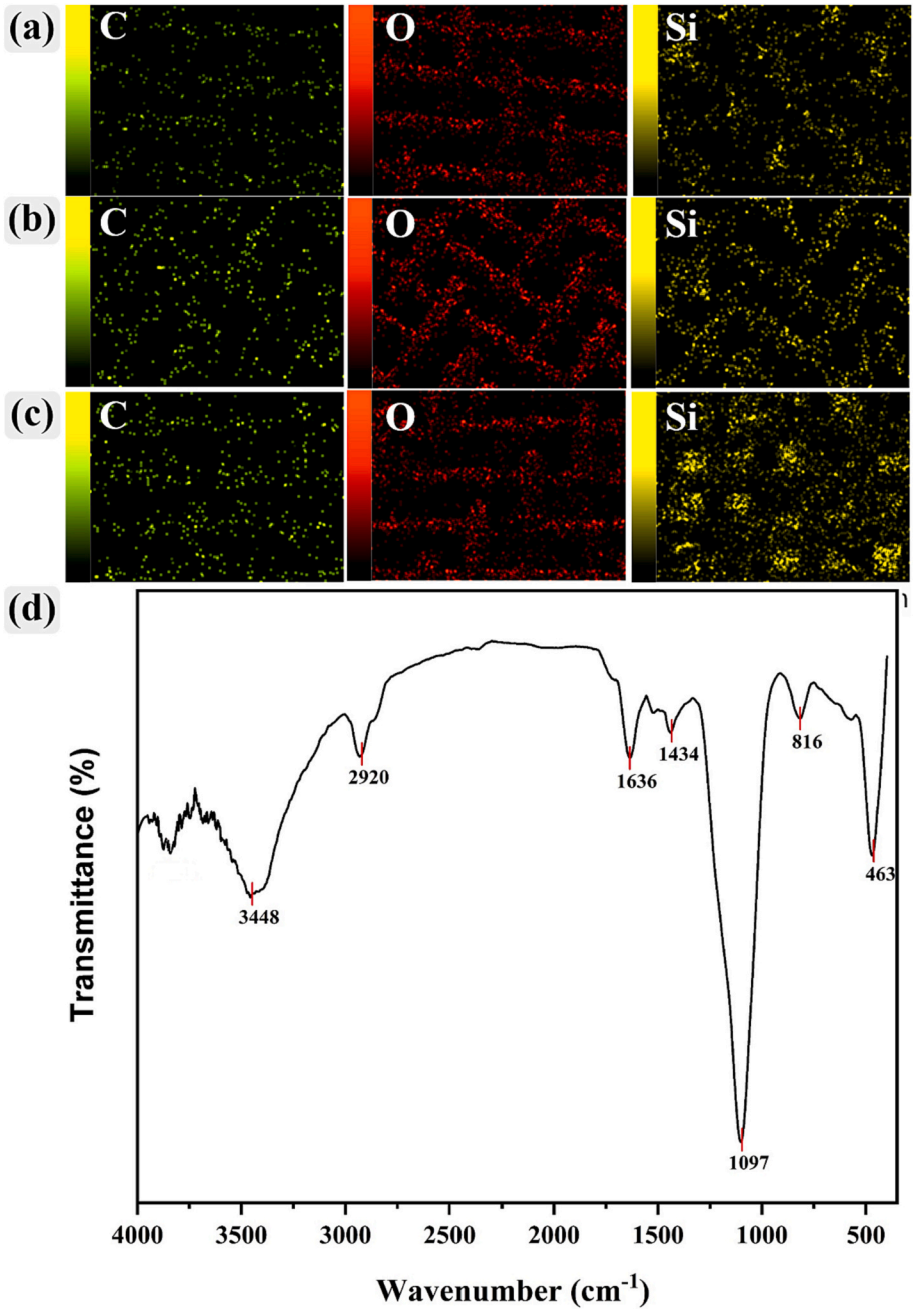

Fig. 3. EDS mapping images of (a) SS-1, (b) SS-2 and (c) SS-3 samples. (d) FTIR spectra of SS-2.

evidence of a network-like structure (Fig. 2g). Although an additional layer of PS and SiO_2 (SS-2) was applied, aggregated silica particles homogeneously covered the mesh surface and produced regular pores having an average pore size of ~25 μm (Fig. 2b). Fig. 2e reveals how nanosized grains of agglomerated silica particles can generate a homogeneous micro- and nano-scale rough structure. The formed dual-scale hierarchical rough structure is evident in the magnified image (Fig. 2h). As a result, this hierarchical rough structure enables air trapping under the water droplet. Meanwhile, micropores of mesh substrate with hydrophobic groups allow it to enter the oil. After applying three layers of PS and SiO_2, the aggregated silica particles were more uniformly dispersed, as depicted in Fig. 2c, f, i. The high-resolution SEM images clearly displayed the presence of micro-nano hierarchical surface morphologies, which are responsible for the superhydrophobicity. Moreover, the complete water-resisting and self-cleaning behaviors on the mesh substrate also proved the occurrence of the Cassie-Baxter state on the substrate (Nagappan and Ha, 2015; Nagappan et al., 2013). Increasing the number of coating layers could increase the surface roughness. In addition, the higher resolution SEM images also display the reduced porosity and pore sizes with the three-layer coating due to the formation of more micro-nano hierarchical particles on the substrate. Among the three, SS-2 exhibited a more uniform coating with high porosity than SS-1 and SS-3. Therefore, SS-2 is considered optimum and used for further characterizations.

Fig. 3(a-c) illustrates the EDS elemental mapping images of the prepared PS-SiO_2 coatings. The one-layer PS-SiO_2 coating (SS-1) contained C, O and Si with mass % of 57.32, 37.96 and 4.72, respectively. The elemental percentage increases for the SS-2 sample with 60.96 % C, 31.85 % O, and 7.19 % Si. The corresponding percentages in the SS-3 sample were 62.90 % C, 26.72 % O and 10.38 % Si. The incorporation of the low surface energy PS (40.7 mJ/m^2) and the hydrophobic SiO_2 particles (50.54 mJ/m^2) could improve the coating's wettability (Roh

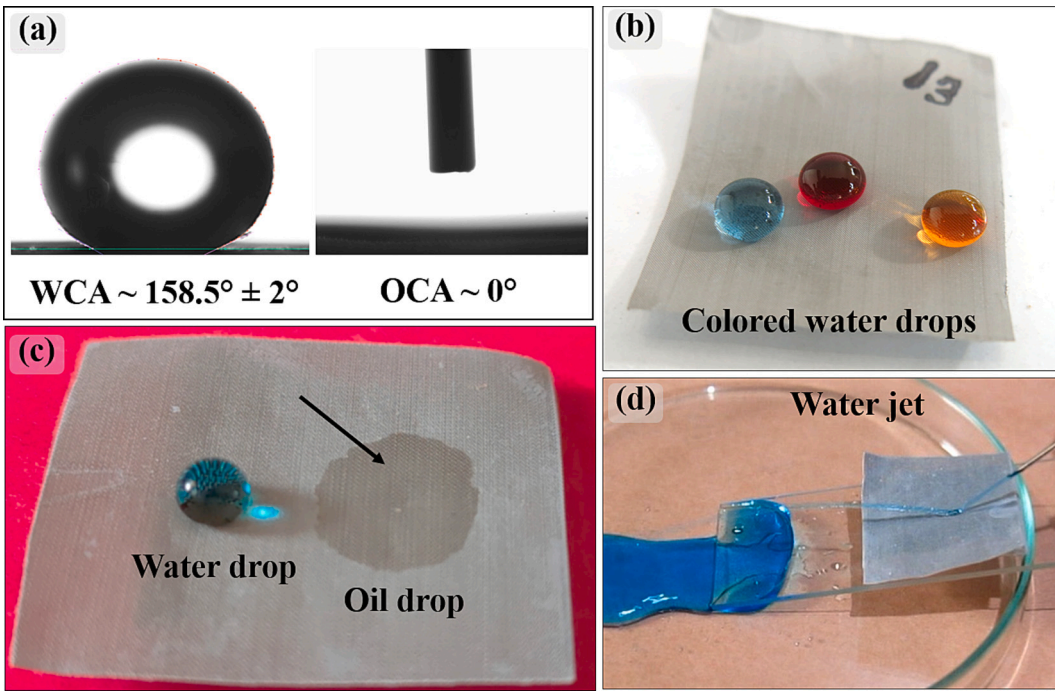

Fig. 4. Optical photograph of (a) Water and oil drops on SS-2 sample collected from contact angle meter, (b) Colored water drops on SS-2 sample, (c) Blue color water drop along with a spread coconut oil drop on SS-2 sample and (d) Screen snap of hitting water jet. (For interpretation of the references to color in this figure legend, the reader is referred to the web version of this article.)

et al., 2014; Kinloch, 1987).

Fig. 3d shows FTIR graph of two-layer PS-SiO_2 coating on steel mesh. The characteristic peaks are appeared in the wavelength range of 400 to 4000 cm^{-1}. The peaks at 3448 cm^{-1} and 1636 cm^{-1} indicate the existence of O—H bonding. The peaks at 2920 cm^{-1} and 1434 cm^{-1} (C—H stretching and bending vibrations) correspond to long-chain alkyl groups on coating surface. (Ren et al., 2020) The strong peak at 1097 cm^{-1} represents Si–O–Si asymmetric stretching vibration (Zhang et al., 2018). The peaks at 816 cm^{-1} and 463 cm^{-1} indicate Si—O bonding. These peaks confirm that the PS and SiO_2 were presented on the coating surface.

3.2. Wettability and oil-water separation capability

The solid-liquid interfacial attraction or repulsion determines surface wettability. The water/oil contact angles and water sliding angles on the coated surface were measured using a contact angle meter. The WCA for the SS-1 sample was estimated to be 146.5° ± 2° and SA was 19° ± 1°. As shown in Fig. 4a, the SS-2 sample exhibited a WCA of 158.5° ± 2° and OCA (coconut oil) of around 0°, attributed to the micro- and nano-scale hierarchical surface roughness offered by the two-layer coating. The water drops rolled down when the mesh was turned at a 5° ± 1° angle (a movie file (Movie S6) showing the rolling behavior of water droplet on the coated mesh surface is provided in the supplementary information). The WCA and SA of the SS-3 sample was 152.2° ± 2° and 9° ± 1°, respectively. The decrease of WCA could be due to the more compactly deposited SiO_2 particles. Fig. 4b depicts the colored water drops on the superhydrophobic SS-2 mesh. As depicted in Fig. 4c, the SS-2 sample could completely absorb the coconut oil while repelling water droplets. Water jet impact was used to test the coating stability to striking water jets. The continuous water jet was produced using a 20 mL syringe and hit on the SS-2 sample at a precise location. Even after 2 min of impacting, the water jet repels in the opposite direction from the impacting point (Fig. 4d).

Reverse wetting properties of coated mesh towards water and oil facilitated the separation of the oil-water mixture. Mesh pore size and porosity are crucial factors in determining the separation efficiency. When separating an oil-water mixture, the mesh surface will absorb the oil phase, making it oil-wetted. The oil-wetted surface will then strongly repel the water phase. Due to its porous structure, the oil phase can pass through the mesh while separating from the water phase.

The SS-2 mesh was tested for oil-water separation using the pre-designed mesh bucket and various oil-water mixtures of 75 mL of water and 75 mL of various oils, including petrol, diesel, kerosene, vegetable oil, and coconut oil. As shown in Fig. 5a, highly adhesive glue was used to secure the fabricated SS-2 sample to the top of a 100 mL plastic bucket. The bucket provides space to gather oil filtrated from superhydrophobic mesh. A diagrammatic representation of oil collection is shown in Fig. 5b. For example, the mixture of petrol oil and green-colored dyed water was separated. When the separation apparatus was submerged in an oil and water mixture, the porous structure of SS-2 mesh allowed oil to pass through but prevented water from passing (see Fig. 5c, step-1 & 2). After oil was collected in the plastic bucket designated for oil collection, the bucket was removed, and oil was poured into a different glass beaker (see Fig. 5c, step-3 & 4). This procedure was carried out a maximum of three times to complete the oil-water separation. The separation process of various oil-water mixtures is visualized in Movie S1 to Movie S5. Fig. 5d schematically illustrates the potential for large-scale application of the superhydrophobic SS mesh bucket.

Separation efficiency (η) is an essential factor when utilizing superhydrophobic mesh for real applications. The separation efficiency was calculated using the following equation: η = [volume of water after separation (v) / volume of water before separation (v_0)] x 100 % (Zhu et al., 2020). The effectiveness of separating oil-water mixtures depends on the viscosity of the oils. In separation experiments, the SS-2 sample showed 99.33 % efficiency for low viscous oil and 86.66 % of efficiency for high viscous oil (Fig. 6a). Low-viscosity oil has lower molecular density, which allows for greater molecular mobility. On the other hand, high-viscosity oil has a higher molecular density, resulting in lower molecular mobility. High-viscosity oil (vegetable) causes poor fuel atomization, large droplet size and kinematic viscosities to be 7 to 10

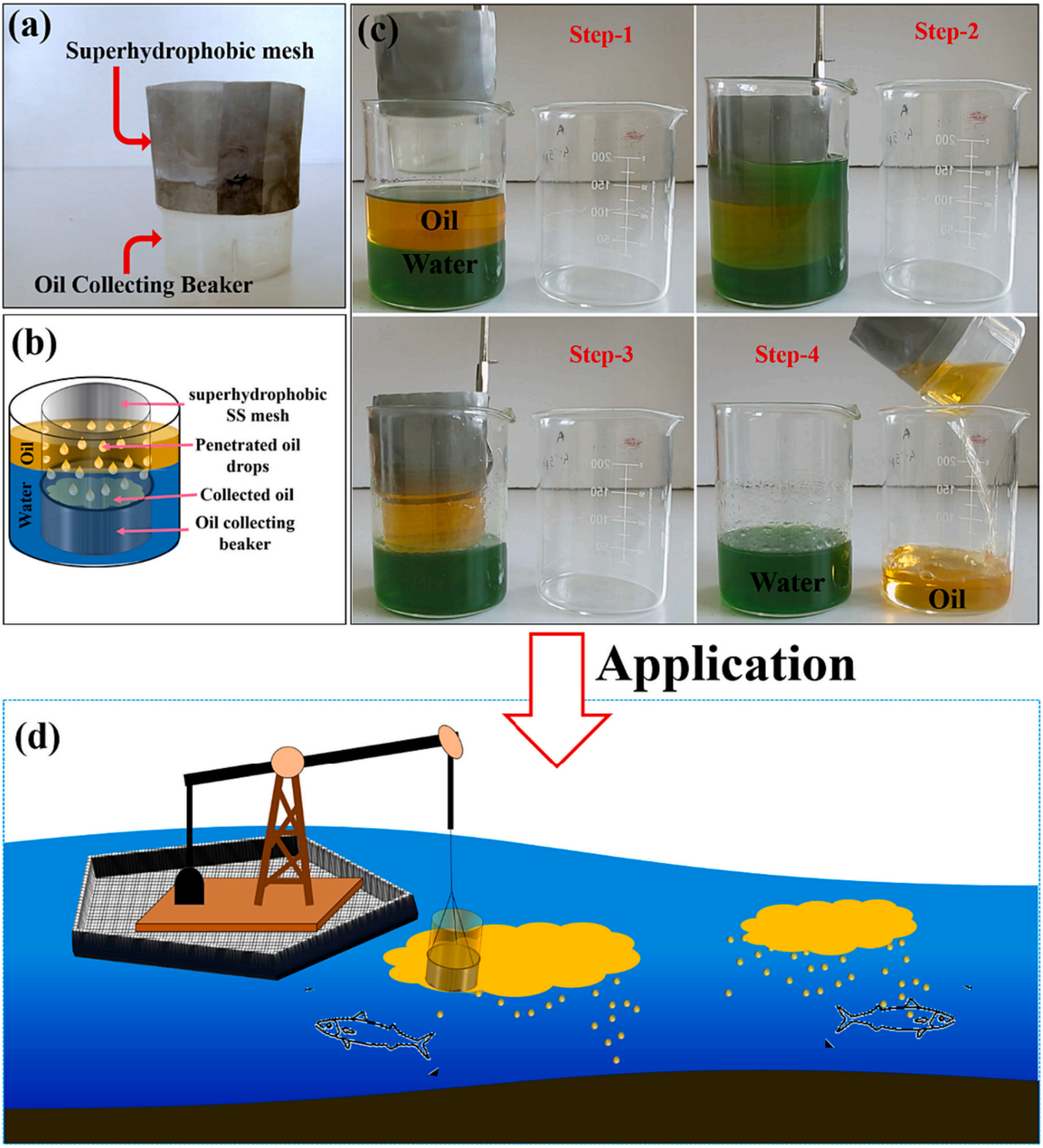

Fig. 5. (a) The image of the oil-water separation setup, (b) Schematic of oil collection by oil-water separation setup, (c) Step-1 to Step-4 displayed oil-water mixture separation process. (d) A schematic showing the practical application of the superhydrophobic mesh bucket.

times higher than diesel. Vegetable oil has densities of 12 % to 15 % higher than diesel (Sisi et al., 2020; Agarwal et al., 2008). Low viscous oil can pass through micropores of superhydrophobic stainless steel mesh under gravity. Conversely, highly viscous oil adheres to mesh and pore walls and forms a bridge between the walls of microspores, which impedes flow. Hence, high viscous oil shows less separation effectiveness than low viscous oil.

In the more precise study of the oil-water mixture separation ability of the mesh bucket, the oil-water mixture was prepared by adding 10 mL of oil to 100 mL of water. The as-prepared superhydrophobic mesh was submerged into the oil-water mixture and the gathered oil in the plastic bucket was collected; the separation process was repeated three times. As shown in Fig. 6b, the mesh bucket revealed >99 % separation efficiency for low viscous oils and >85 % for high viscous oils. We have further studied the reusing ability of the mesh bucket using diesel-water mixtures. After each cycle, the mesh was dried in hot air and reused for the separation. Notably, superhydrophobic mesh exhibited outstanding separation ability (>98 %) even after 30 cycles of reuse (Fig. 6c). To evaluate the effectiveness of mesh buckets in separating an oil-water mixture with low oil content, 1 mL of oil was mixed with 100 mL of water. When a superhydrophobic mesh bucket was submerged in an oil-water mixture, the mesh bucket absorbs the oil from water, but cannot

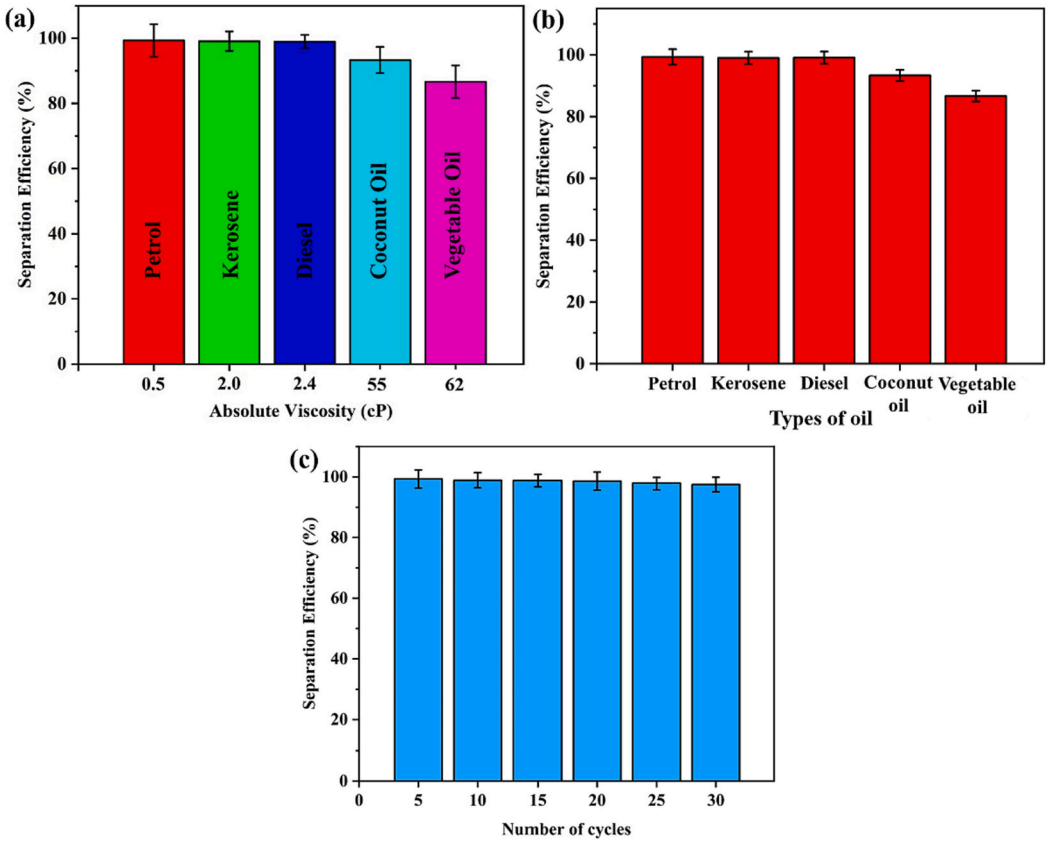

Fig. 6. Oil-water separation efficiency with different viscous oils, (a) for 50 % and (b) for 10 % of oil in water mixtures. (c) Variation of separation efficiency with number of separation cycles.

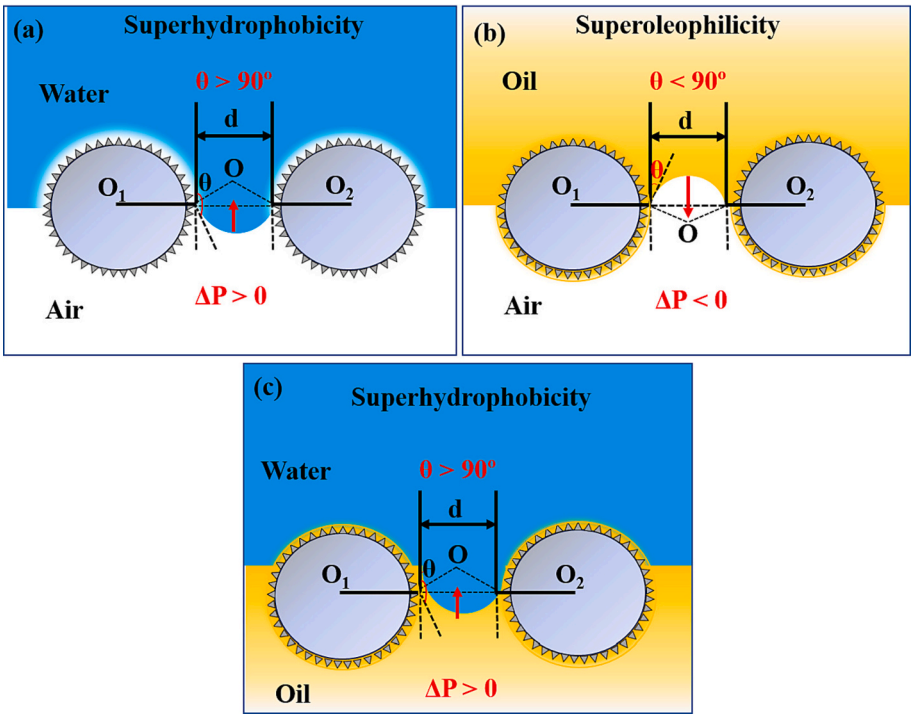

Fig. 7. Schematic diagrams demonstrating the oil-water separation mechanism. (a) Superhydrophobic mesh and $\Delta p > 0$ in water, (water cannot pass through the mesh), (b) Superoleophilic mesh and $\Delta p < 0$ in oil (permeable to oil), and (c) Superhydrophobic mesh and $\Delta p > 0$ in oil-water mixture (water can stay above the mesh). O is the center of the capillary, O_1 and O_2 are the cross-section centers of the mesh wire, and R is the radius of curvature of the meniscus.

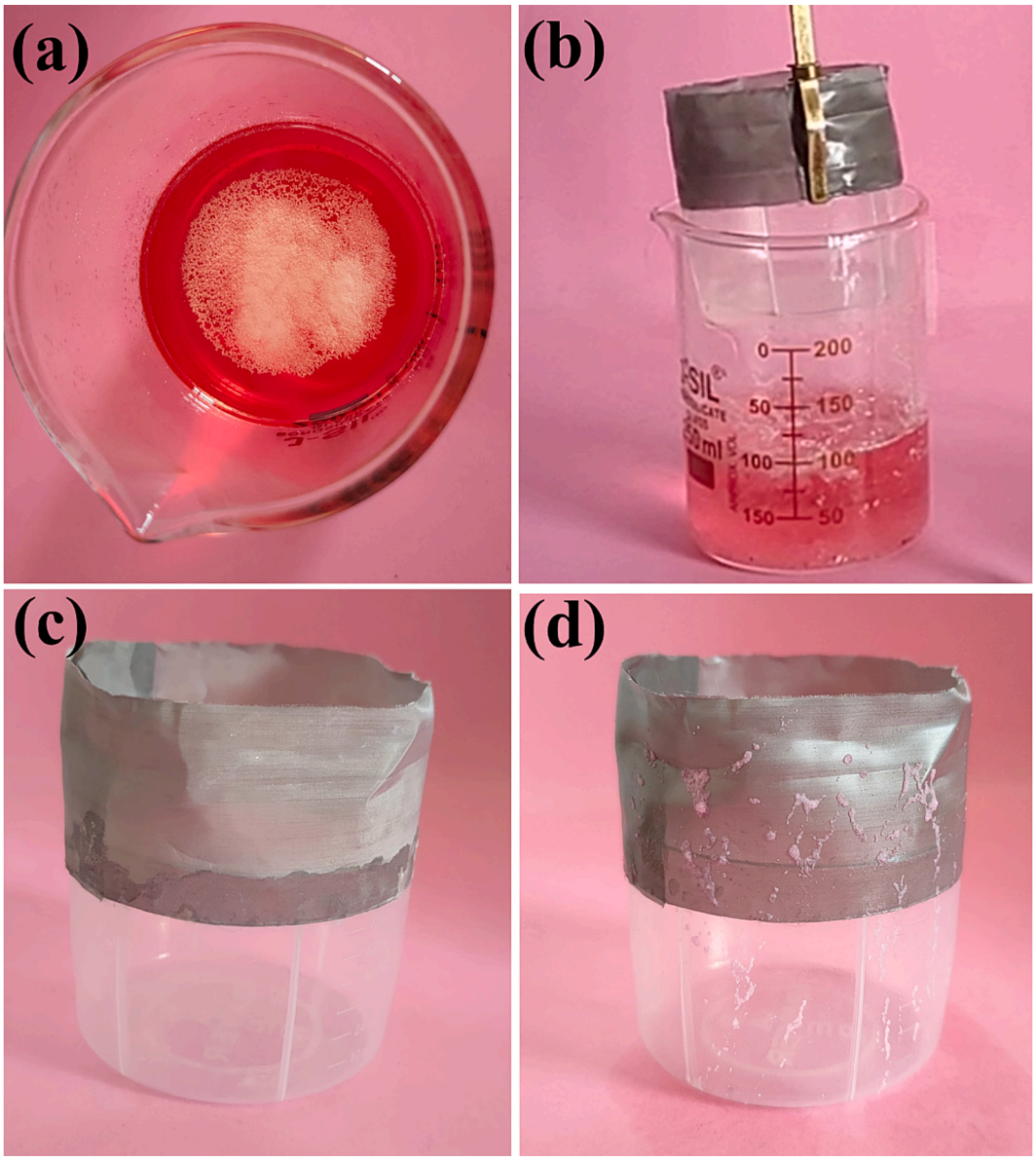

Fig. 8. (a) Microplastics dispersion in the mixture of hexane and aqueous NaCl solution, (b) microplastics separation process, (c) mesh bucket before separation, and (b) after separation microplastic particles stained on the mesh bucket surface.

be collected in a bucket. It is concluded that the as-prepared mesh bucket can effectively separate oil-water mixture with high oil content, but it cannot be used to separate oil from water having low content of oil (minimum volume of oil required to wet mesh surface). These results evidenced the excellent oil-water separation ability of the developed mesh bucket for both large and small amounts of oil content and its reusability.

3.3. Oil-water separation mechanism

The mesh bucket is capable of effectively separating oil and water due to its superhydrophobic-superoleophilic properties. We analyzed the oil-water separation mechanism using the special wetting property of mesh for better understanding. The bare mesh was hydrophobic and oleophobic. After depositing PS and SiO_2 layers, the surface roughness was varied, with the associated surface energy lowering due to PS. This improves surface wettability by the capillary effect based on the Wenzel equation (Wenzel, 1936).

$$\mathrm{Cos}\ \theta = \mathrm{r}\ \mathrm{Cos}\ \theta_1 \quad (1)$$

where r is the roughness factor, θ and θ_1 are the WCAs, respectively, on coated and original meshes. According to Wenzel equation, if θ_1 is $>90^\circ$, the θ increases with r and is greater than θ_1. In this study, PS and SiO_2 covered mesh has showed WCA (θ) of $158.5^\circ \pm 2^\circ$, which is significantly higher than the WCA (θ_1) of original mesh ($84^\circ \pm 2^\circ$). The WCAs where measured immediately after depositing water droplets.

In addition, when the surface is rough, air pockets become entangled, preventing liquid from being pinned into the surface cavity. The surface forms a solid-liquid-air interface, which can be explained by the Cassie-Baxter formula (Liu et al., 2009).

$$\mathrm{Cos}\ \theta = \mathrm{f}\ \mathrm{Cos}\ \theta_1 + \mathrm{f}{-}1 \quad (2)$$

where f is the fraction of contact area of solid mesh with water. In this study, $\theta = 158.5^\circ \pm 2^\circ$, $\theta_1 = 84^\circ \pm 2^\circ$ and f = 0.06301, indicating that only 6.301 % area of the liquid droplet was in contact with the mesh surface. The higher WCA of coated mesh corresponds to a lesser contact area of the water droplets with the mesh surface. Fig. 7 represents a schematic model that can help us understand the process of separating

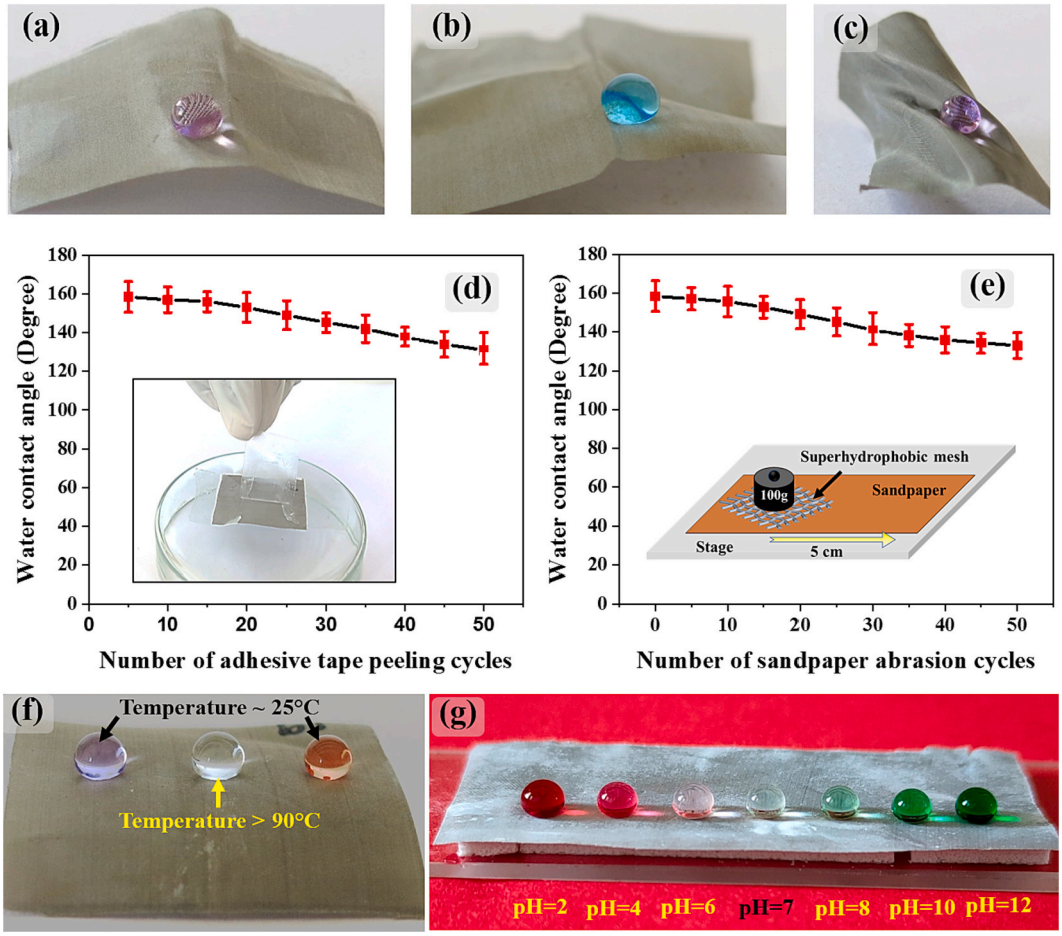

Fig. 9. (a) Bending, (b) Folding and (c) Twisting of SS-2 sample. Variation of WCA with (d) Tape peeling test and (e) Sandpaper abrasion test on SS-2 sample. Optical image of (f) Hot and normal water drops and (g) Colored drops with pH 2 to 12 on SS-2 sample.

oil and water. The theoretical intrusion pressure (P) is calculated using Eq. (3) (Ma et al., 2018).

$$P = (2\gamma_{12})/R = -l\,\gamma_{12}\,\mathrm{Cos}\,\theta_A/A \quad (3)$$

where, γ_{12} is the water/oil interfacial surface tension, θ_A is the WCA of the superhydrophobic mesh, R is the radius of the meniscus, l is the pore's circumference and A is the cross-sectional area of the pore. Considering the superhydrophobic mesh in air, $\theta_A > 90°$ then $\Delta P > 0$, in this case, the superhydrophobic mesh can withstand the pressure, and water cannot permeate (Fig. 7a). In Fig. 7b, the superoleophilic mesh in air, $\theta A < 90°$ then $\Delta P < 0$; in this case, oil will penetrate into the superoleophilic mesh. Conversely, when mesh was wetted by oils, the oil was trapped in the rough structure, strengthening the water-repellency force. Consequently, $\theta_A > 90°$ and $\Delta P > 0$, can sustain the degree of pressure (Fig. 7c). After oil permeation, water can be retained above the mesh surface, enabling successful separation of oil-water mixture using the prepared superhydrophobic/superoleophilic mesh bucket.

3.4. Microplastic removal capability

The superhydrophobic mesh bucket's ability to remove microplastics was tested using PVC microparticles as pollutants. The PVC microplastics (20 mg) were dispersed in 2 wt% NaCl aqueous solution (100 mL of water). Next, hexane (10 mL) was added to the solution and stirred gently. The aqueous solution was colored with red dye to differentiate between the aqueous and organic (oil) phases. While stirring, microplastic particles moved from the water phase to the water-hexane interface as they have a higher affinity to hexane than water (Fig. 8a). A similar separation procedure as described above was used. The microplastic separation device is shown in Fig. 8b.

When the oil phase comes into contact with the superhydrophobic/superoleophilic mesh, it gets absorbed and passes through the mesh, while water droplets are repelled. During the separation process, microplastic particles stick to the mesh bucket's surface, and particles smaller than the mesh's pore size can pass through it with hexane and be collected in the oil collector bucket. After the separation, the mesh bucket was dried at 55 °C in hot air oven for 10 min. Fig. 8c and d shows the mesh bucket surface before and after separation. The surface is clean before separation, but microplastic particles adhere to the surface after separation. The weight of the microplastic particles adhered to the mesh bucket and those collected in the beaker were measured. To evaluate the microplastic removal efficiency of the mesh bucket, the following relation was used: Microplastic removal efficiency (%) = $[M_1/M_0]$ x 100, where M_0 is the weight of PVC microparticles used for the experiment and M_1 is the mass of the PVC powder adhered to the mesh bucket and collected in the beaker. The mesh bucket removed 19 g of microplastics, resulting in 95 % microplastic removal efficiency.

3.5. Mechanical, chemical and thermal durability

Before utilizing functional materials in real-life scenarios, it is essential to test their mechanical durability. The superhydrophobic mesh underwent rigorous testing, including bending, folding, and twisting (Jeong et al., 2010), adhesive tape peeling (Jung et al., 2018) and rubbing on sandpaper (Huang et al., 2021), to assess its mechanical strength. The SS-2 sample was bent at different angles, folded in

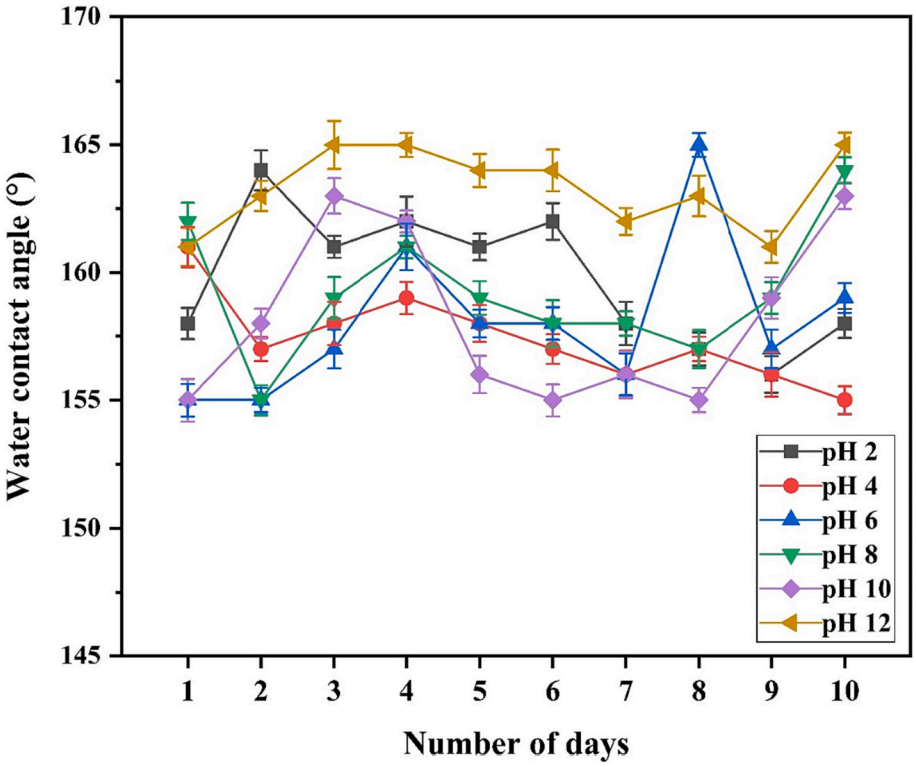

Fig. 10. Variation of WCA with number of days of immersion in different pH solutions.

different directions, and twisted at different angles and directions. The affected mesh was quickly tested for WCA and SA, revealing that it's wetting properties remained unchanged. Even after being bent, folded, and twisted over 30 times, the mesh maintained its superhydrophobic properties with WCA > 154° and SA < 6° (Fig. 9a-c). The adhesive tape test was performed on SS-2 samples. The tape peeling tests were executed by carefully detaching the tape from the firmly attached SS-2 mesh. The WCA was measured on the tape-detached part of the mesh. A single cycle of the tape peeling test had no impact on the WCA. The mesh retained its superhydrophobic properties (WCA > 152° and SA < 7°) even after undergoing a tape peeling test for 25 cycles. After running for over 30 cycles, the water droplet remained on the mesh surface, and its WCA was approximately 143.2° ± 1°. However, after 30 cycles, the mesh's superhydrophobic properties were lost, and the WCA significantly decreased. After 50 cycles of tape peeling tests, the WCA dropped to 132.6° ± 2° and water droplets stuck to surface (Fig. 9d). The reason for this could be that the coating's surface structure has vanished. The sandpaper abrasion test was conducted like the one described in the literature (Wang et al., 2020). Sandpaper was placed under the SS-2 mesh mounted on a micro-glass slide. It was loaded with 100 g and dragged over sandpaper at a consistent speed (5 mm s^{-1}) for 10 cm for one cycle. The sandpaper abrasion tests (Fig. 9e) indicate that the SS-2 mesh retains its superhydrophobic properties (WCA > 151° and SA < 8°) even after being abraded for 20 cycles. After 50 cycles, however, the WCA decreased to 137.8° ± 2° and water droplets adhered to coating surface. Coatings may get damaged due to mechanical abrasion; consequently, the coating loses superhydrophobic properties. This investigation concluded that the proposed mesh bucket sample could retain its superhydrophobic properties after bending, folding, twisting, tape peeling, and sandpaper abrasion.

In severe circumstances, the superhydrophobic mesh must exhibit chemical and thermal stability. To determine the thermal stability of the SS-2 sample, it was heated from 100 °C to 300 °C for 1 h, and in another method of testing, a hot water drop was placed on it (Huang et al., 2021). The heating studies showed that the WCA of mesh slightly change and maintained its superhydrophobicity with WCA of 155° and 6° of SA until a temperature of 200 °C. The WCA, however, decreased to 143.4° ± 2° after raising the temperature further, which may be caused by the degradation of the hydrophobic group on the coating surface. After heating at 300 °C, the mesh had a WCA below 140.5° ± 3°, indicating that the hydrophobic groups were completely lost. In the hot water drop test, when the droplet at around 90 °C was placed on the SS-2 sample, it was shaped into a sphere akin to a regular water droplet, as shown in Fig. 9f.

The chemical stability of the SS-2 sample was evaluated by depositing drops of different pH solutions on the surface (Vanithakumari et al., 2021), and in another method, the sample was immersed in solutions having different pH for 10 days (Li et al., 2021). The CA of the droplets of colored solutions with pH in the range of 2 to 12 were measured. As depicted in Fig. 9g, different pH solution droplets had spherical shapes with CA > 152°. The direct immersion studies showed that the CA was slightly altered after 10 days of immersion in pH 2 to 12 solutions; however, the sample retained the superhydrophobicity with WCA > 155° and SA < 6°. The variation of WCA with number of day's immersion in different pH solutions is shown in Fig. 10. The high chemical stability is influenced by the micro- and nano-scale rough surface structure and low surface energy molecules (Zhao et al., 2022). The presence of SiO_2 nanoparticles in the coating could enhance the stability due to their chemical inertness (Sriram et al., 2020; Li et al., 2019). The marginal variation of the WCA observed during the chemical durability studies can be due to the wet chemical etching, which may detach SiO_2 nanoparticles from PS and SiO_2 nanoparticles layer coatings and other adsorbed coating components and hence alter the surface roughness and surface energy. Also, with time, the surface roughness and morphology likely varied, which may result in a marginal increase or decrease in the contact angle.

4. Conclusions

We have successfully developed a superhydrophobic stainless steel

mesh bucket by layer coatings of polystyrene and SiO_2 nanoparticles. A facile approach for oil-water separation using the superhydrophobic mesh bucket was illustrated. The surface and chemical structural analysis confirmed the existence of a hierarchical roughened surface with low surface energy molecules on the coating surface. As a result, the prepared superhydrophobic mesh has exhibited WCA of 158.5° ± 2°, OCA of nearly 0°, and a SA of 5° ± 1°. The oil-water separation tests conducted with the superhydrophobic mesh bucket showed that it could effectively separate low viscous oil with a 99.33 % efficiency and high viscous oil with 86.66 % efficiency. Additionally, the mesh bucket had showed ~95.0 % microplastics removal efficiency. The mesh coating's superhydrophobicity remained intact even after undergoing mechanical durability tests, such as 30 times of bending, folding, and twisting, 25 times of tape tearing, and 20 times abrasion on sandpaper. The coating remained stable even if the mesh was heated to 200 °C or hot water drops were placed on it. It was also durable when dipped in different pH solutions (pH 2–12) for 10 days or dropped different pH solutions on the mesh surface. The facile fabrication approach of the oil-water separating mesh bucket described in this work has the potential to be commercially used in various application areas.

Supplementary data to this article can be found online at https://doi.org/10.1016/j.marpolbul.2023.115790.

CRediT authorship contribution statement

Rajaram S. Sutar: Conceptualization, Methodology, Investigation, Writing - original draft. **Sanjay S. Latthe:** Supervision, Writing – review & editing, Visualization. **Akshay R. Jundle:** Methodology, Investigation. **Pradip P. Gaikwad:** Methodology, Investigation. **Sagar S. Ingole:** Methodology, Investigation. **Saravanan Nagappan:** Formal analysis, Writing – review & editing. **Yong Hyun Kim:** Validation, Writing - review & editing. **Appasaheb K. Bhosale:** Validation, Formal analysis. **Viswanathan S. Saji:** Validation, Writing - review & editing. **Shanhu Liu:** Supervision.

Declaration of competing interest

The authors declare that they have no known competing financial interests or personal relationships that could have appeared to influence the work reported in this paper.

Data availability

The data that has been used is confidential.

Acknowledgments

We greatly appreciate the support of the National Natural Science Foundation of China (21950410531), and the support of the Petro-China Research Institute of Petroleum Exploration & Development (RIPED-2019-CL-186). This work is financially supported by DST – INSPIRE Faculty Scheme, Department of Science and Technology (DST), Govt. of India [DST/INSPIRE/04/2015/000281].

References

Agarwal, D., Kumar, L., Agarwal, A.K., 2008. Performance evaluation of a vegetable oil fuelled compression ignition engine. Renew. Energy 33 (6), 1147–1156.
Baig, U., Gondal, M., Dastageer, M., 2022. Oil-water separation using surface engineered superhydrophobic and superoleophilic membrane for the production of clean water. J. Water Process Eng. 45, 102473.
Barron, M.G., Vivian, D.N., Heintz, R.A., Yim, U.H., 2020. Long-term ecological impacts from oil spills: comparison of Exxon Valdez, Hebei Spirit, and Deepwater Horizon. Environ. Sci. Technol. 54 (11), 6456–6467.
Bolvardi, B., Seyfi, J., Hejazi, I., Otadi, M., Khonakdar, H.A., Davachi, S.M., 2019. Towards an efficient and durable superhydrophobic mesh coated by PDMS/TiO_2 nanocomposites for oil/water separation. Appl. Surf. Sci. 492, 862–870.
Chen, J., Wu, J., Zhong, Y., Ma, X., Lv, W., Zhao, H., Zhu, J., Yan, N., 2023. Multifunctional superhydrophilic/underwater superoleophobic lignin-based polyurethane foam for highly efficient oil-water separation and water purification. Sep. Purif. Technol. 311, 123284.
Dalawai, S.P., Aly, M.A.S., Latthe, S.S., Xing, R., Sutar, R.S., Nagappan, S., Ha, C.S., Sadasivuni, K.K., Liu, S., 2020. Recent advances in durability of superhydrophobic self-cleaning technology: a critical review. Prog. Org. Coat. 138, 105381.
Gong, H., Yu, B., Dai, F., Peng, Y., 2018. Influence of electric field on water-droplet separated from emulsified oil in a double-field coupling device. Colloids Surf. A Physicochem. Eng. Asp. 550, 27–36.
Guo, D., Hou, K., Xu, S., Lin, Y., Li, L., Wen, X., Pi, P., 2018. Superhydrophobic-superoleophilic stainless steel meshes by spray-coating of a POSS hybrid acrylic polymer for oil-water separation. J. Mater. Sci. 53, 6403–6413.
Guo, Y., Zhou, X., Yi, X., Wang, D., Xu, Q., 2020. Superhydrophobic behaviors of nano SiO_2 coating on stainless steel mesh and its application in oil/water separation. Appl. Nanosci. 10, 1511–1520.
Gupta, S., Tai, N.H., 2016. Carbon materials as oil sorbents: a review on the synthesis and performance. J. Mater. Chem. A 4, 1550–1565.
He, Z., Wu, H., Shi, Z., Kong, Z., Ma, S., Sun, Y., Liu, X., 2022. Facile preparation of robust superhydrophobic/superoleophilic TiO_2-decorated polyvinyl alcohol sponge for efficient oil/water separation. ACS Omega 7 (8), 7084–7095.
Huang, J., Li, M., Lu, Y., Ren, C., Wang, S., Wu, Q., Li, Q., Zhang, W., Liu, X., 2021. A facile preparation of superhydrophobic L-CNC-coated meshes for oil–water separation. RSC Adv. 11, 13992–13999.
Hwang, H.S., Kim, N.H., Lee, S.G., Lee, D.Y., Cho, K., Park, I., 2011. Facile fabrication of transparent superhydrophobic surfaces by spray deposition. ACS Appl. Mater. Interfaces 3 (7), 2179–2183.
Jeong, H.E., Kwak, M.K., Suh, K.Y., 2010. Stretchable, adhesion-tunable dry adhesive by surface wrinkling. Langmuir 26 (4), 2223–2226.
Ji, H., Zhao, R., Li, Y., Sun, B., Li, Y., Zhang, N., Qiu, J., Li, X., Wang, C., 2018. Robust and durable superhydrophobic electrospun nanofibrous mats via a simple Cu nanocluster immobilization for oil-water contamination. Colloids Surf. A Physicochem. Eng. Asp. 538, 173–183.
Jung, D., Kim, J.A., Park, M.-S., Yim, U.H., Choi, K., 2017. Human health and ecological assessment programs for Hebei Spirit oil spill accident of 2007: status, lessons, and future challenges. Chemosphere 173, 180–189.
Jung, K.K., Jung, Y., Choi, C.J., Ko, J.S., 2018. Highly reliable superhydrophobic surface with carbon nanotubes immobilized on a PDMS/adhesive multilayer. ACS Omega 3 (10), 12956–12966.
Kinloch, A.J., 1987. Adhesion and Adhesives: Science and Technology. Springer Science & Business Media, p. 25.
Kumari, P., Chauhan, P., Kumar, A., 2022. Superwetting Materials for Modification of Meshes for Oil/WATER Separation, Oil-water Mixtures and Emulsions, Volume 2: Advanced Materials for Separation and Treatment. American Chemical Society, pp. 1–23.
Latthe, S.S., Sutar, R.S., Shinde, T.B., Pawar, S.B., Khot, T.M., Bhosale, A.K., Sadasivuni, K.K., Xing, R., Mao, L., Liu, S., 2019. Superhydrophobic leaf mesh decorated with SiO_2 nanoparticle-polystyrene nanocomposite for oil–water separation. ACS Appl. Nano Mater. 2 (2), 799–805.
Li, B., Miller, R.H., Zhang, H., Ouyang, Y., Qiu, R., Hu, S., Niu, H., 2021. A facile one-step route to fabricate bio-inspired superhydrophobic matrix with high corrosion inhibition to Cumetal. Surf. Interfaces 5, 101189.
Li, F., Kong, W., Zhao, X., Pan, Y., 2020. Multifunctional TiO_2-based superoleophobic/superhydrophilic coating for oil–water separation and oil purification. ACS Appl. Mater. Interfaces 12 (15), 18074–18083.
Li, J., Zhao, Z., Zhang, Y., Li, M., Luo, Z., Luo, L., 2017. Facile fabrication of superhydrophobic SiO_2-coated mesh used for corrosive and hot water/oil separation. J. Sol-Gel Sci. Technol. 82, 299–307.
Li, X., Peng, Y., Zhang, F., Yang, Z., Dong, Z., 2022. Fast-response, no-pretreatment, and robustness air-water/oil amphibious superhydrophilic-superoleophobic surface for oil/water separation and oil-repellent fabrics. Chem. Eng. J. 427, 132043.
Li, Y., Zhang, R., Yu, H., Chen, G., Zhu, M., Qiu, B., Zou, H., Li, X., 2019. Fluorinated nanosilica size effect on hierarchical structure and superhydrophobic properties of the epoxy nanocomposite film. ACS Appl. Polym. Mater. 2 (2), 418–426.
Liu, M., Wang, S., Wei, Z., Song, Y., Jiang, L., 2009. Bioinspired Design of a Superoleophobic and low Adhesive Water/solid Interface. Adv. Mater. 21, 665–669.
Lü, X., Lin, H., 2021. Facile fabrication of robust superhydrophobic/superoleophlic Cu coated stainless steel mesh for highly efficient oil/water separation. Sep. Purif. Technol. 256, 117512.
Ma, W., Zhang, M., Liu, Z., Huang, C., Fu, G., 2018. Nature-inspired creation of a robust free-standing electrospun nanofibrous membrane for efficient oil–water separation. Environ. Sci. Nano 5 (12), 2909–2920.
Nagappan, S., Ha, C.S., 2015. Emerging trends in superhydrophobic surface based magnetic materials: fabrications and their potential applications. J. Mater. Chem. A 3 (7), 3224–3251.
Nagappan, S., Park, J.J., Park, S.S., Lee, W.K., Ha, C.S., 2013. Bio-inspired, multi-purpose and instant superhydrophobic–superoleophilic lotus leaf powder hybrid micro–nanocomposites for selective oil spill capture. J. Mater. Chem. A 1 (23), 6761–6769.
Pan, Y., Huang, S., Li, F., Zhao, X., Wang, W., 2018. Coexistence of superhydrophilicity and superoleophobicity: theory, experiments and applications in oil/water separation. J. Mater. Chem. A 6, 15057–15063.
Phan, N.M., Kim, J.-H., Kim, J., Weon, B.M., Yi, G.-R., 2021. Durable tetra-scale superhydrophobic coatings with virus-like nanoparticles for oil–water separations. Appl. Surf. Sci. 570, 151088.
Qu, M., Ma, L., Zhou, Y., Zhao, Y., Wang, J., Zhang, Y., Zhu, X., Liu, X., He, J., 2018. Durable and recyclable superhydrophilic-superoleophobic materials for efficient oil/

water separation and water-soluble dyes removal. ACS Appl. Nano Mater. 1 (9), 5197–5209.
Ren, H.T., Cai, C.C., Cao, W.B., Li, D.S., Li, T.T., Lou, C.W., Lin, J.H., 2023. Superhydrophobic TiN-coated cotton fabrics with nanoscale roughness and photothermal self-healing properties for effective oil–water separation. ACS Appl. Nano Mater. 6 (13), 11925–11933.
Ren, T., Tang, G., Yuan, B., Yang, Y., Yan, Z., Ma, L., Huang, X., 2020. Hexadecyltrimethoxysilane-modified SiO_2 nanoparticle-coated halloysite nanotubes embedded in silicone–acrylic polymer films as durable fluorine-free superhydrophobic coatings. ACS Appl. Nano Mater. 3 (6), 5807–5815.
Rius-Ayra, O., Biserova-Tahchieva, A., Llorca-Isern, N., 2022a. Removal of dyes, oils, alcohol, heavy metals and microplastics from water with superhydrophobic materials. Chemosphere 137148.
Rius-Ayra, O., Biserova-Tahchieva, A., Sansa-López, V., Llorca-Isern, N., 2022b. Superhydrophobic PDMS coated 304 stainless-steel mesh for the removal of HDPE microplastics. Prog. Org. Coat. 170, 107009.
Rius-Ayra, O., Biserova-Tahchieva, A., Sansa-López, V., Llorca-Isern, N., 2022c. Superhydrophobic 304 stainless steel mesh for the removal of high-density polyethylene microplastics. Langmuir 38 (18), 5943–5953.
Roh, S.C., Choi, E.Y., Choi, Y.S., Kim, C.K., 2014. Characterization of the surface energies of functionalized multi-walled carbon nanotubes and their interfacial adhesion energies with various polymers. Polymer 55 (6), 1527–1536.
Sajid, M., Ihsanullah, I., Khan, M.T., Baig, N., 2022. Nanomaterials-based adsorbents for remediation of microplastics and nanoplastics in aqueous media: a review. Sep. Purif. Technol. 122453.
Saththasivam, J., Loganathan, K., Sarp, S., 2016. An overview of oil–water separation using gas flotation systems. Chemosphere 144, 671–680.
Sisi, M.J., Ahmed, M.R., Rohindra, D., 2020. Performance and emission characteristics of a diesel engine employing straight vegetable oils from Vanuatu as fuels. Adv. Mech. Eng. 12 (9), 1687814020962351.
Song, B., 2016. Simple and fast fabrication of superhydrophobic metal wire mesh for efficiently gravity-driven oil/water separation. Mar. Pollut. Bull. 113, 211–215.
Sriram, S., Singh, R.K., Kumar, A., 2020. Silica and Silane based polymer composite coating on glass slide by dip-coating method. Surf. Interfaces 19, 100472.
Vanithakumari, S.C., Athulya, V., George, R.P., Philip, J., 2021. Fabrication of superhydrophobic and self-cleaning PVA-silica fiber coating on 304L SS surfaces by electrospinning. J. Appl. Polym. Sci. 138 (13), 50118.
Velayi, E., Norouzbeigi, R., 2020. A mesh membrane coated with dual-scale superhydrophobic nano zinc oxide: efficient oil-water separation. Surf. Coat. Technol. 385, 125394.
Wang, J., Xu, J., Chen, G., Lian, Z., Yu, H., 2020. Reversible wettability between underwater superoleophobicity and superhydrophobicity of stainless steel mesh for efficient oil–water separation. ACS Omega 6 (1), 77–84.
Wang, X., Yu, P., Zhang, K., Wu, M., Wu, Q., Liu, J., Yang, J., Zhang, J., 2019. Superhydrophobic/superoleophilic cotton for efficient oil–water separation based on the combined octadecanoyl chain bonding and polymer grafting via surface-initiated ATRP. ACS Appl. Polym. Mater. 1 (11), 2875–2882.
Wang, Y., Liu, X., Zhang, H., Zhou, Z., 2015. Superhydrophobic surfaces created by a one-step solution-immersion process and their drag-reduction effect on water. RSC Adv. 5 (24), 18909–18914.
Wenzel, R.N., 1936. Resistance of solid surfaces to wetting by water. Ind. Eng. Chem. 28, 988–994.
Xiong, W., Li, L., Qiao, F., Chen, J., Chen, Z., Zhou, X., Hu, K., Zhao, X., Xie, Y., 2021. Air superhydrophilic-superoleophobic SiO_2-based coatings for recoverable oil/water separation mesh with high flux and mechanical stability. J. Colloid Interface Sci. 600, 118–126.
Xiu, Y., Hess, D.W., Wong, C., 2008. UV and thermally stable superhydrophobic coatings from sol–gel processing. J. Colloid Interface Sci. 326 (2), 465–470.
Xu, Z., Jiang, D., Wei, Z., Chen, J., Jing, J., 2018. Fabrication of superhydrophobic nano-aluminum films on stainless steel meshes by electrophoretic deposition for oil-water separation. Appl. Surf. Sci. 427, 253–261.
Yao, C.W., Tang, S., Sebastian, D., Tadmor, R., 2020. Sliding of water droplets on micropillar-structured superhydrophobic surfaces. Appl. Surf. Sci. 504, 144493.
Zarghami, S., Mohammadi, T., Sadrzadeh, M., Van der Bruggen, B., 2019. Superhydrophilic and underwater superoleophobic membranes-a review of synthesis methods. Prog. Polym. Sci. 98, 101166.
Zhang, L., Chen, H., Sun, J., Shen, J., 2007. Layer-by-layer deposition of poly (diallyldimethylammonium chloride) and sodium silicate multilayers on silica-sphere-coated substrate-facile method to prepare a superhydrophobic surface. Chem. Mater. 19 (4), 948–953.
Zhang, X., Sun, Y., Mao, Y., Chen, K., Cao, Z., Qi, D., 2018. Controllable synthesis of raspberry-like PS–SiO_2 nanocomposite particles via Pickering emulsion polymerization. RSC Adv. 8 (7), 3910–3918.
Zhao, Y., Huo, M., Huo, J., Zhang, P., Shao, X., Zhang, X., 2022. Preparation of silica-epoxy superhydrophobic coating with mechanical stability and multifunctional performance via one-step approach. Colloids Surf. A Physicochem. Eng. Asp. 653, 129957.
Zhou, B., Bashir, B.H., Liu, Y., Zhang, B., 2021a. Facile construction and fabrication of a superhydrophobic copper mesh for ultraefficient oil/water separation. Ind. Eng. Chem. Res. 60 (22), 8139–8146.
Zhou, D.-L., Yang, D., Han, D., Zhang, Q., Chen, F., Fu, Q., 2021b. Fabrication of superhydrophilic and underwater superoleophobic membranes for fast and effective oil/water separation with excellent durability. J. Membr. Sci. 620, 118898.
Zhu, J., Zhao, F., Peng, T., Liu, H., Xie, L., Jiang, C., 2020. Facile preparation of superhydrophobic metal meshes with micro-hierarchical structure via in situ self-assembly metal-organic framework for efficient oil-water separation. Surf. Coat. Technol. 402, 126344.